A Climatic Trigger for the Giant Troll Pockmark Field in the Northern North Sea

Adriano Mazzini[1], Henrik H. Svensen[1], Carl Fredrik Forsberg [2], Henriette Linge[3], Stein-Erik Lauritzen[3], Haflidi Haflidason[3], Øyvind Hammer[4], Sverre Planke [1,5], Tor Inge Tjelta[6]

(1) CEED, University of Oslo, Oslo, Norway (adriano.mazzini@geo.uio.no)

(2) NGI, Oslo, Norway

(3) University of Bergen, Norway

(4) Natural History Museum, University of Oslo, Norway

(5) VBPR, Oslo, Norway

(6) Statoil, Stavanger, Norway

Abstract

Pockmarks are seafloor craters usually formed during methane release on continental margins. However, the mechanisms behind their formation and dynamics remain elusive. Here we report detailed investigations on one of the World's largest pockmark fields located in the Troll region in the northern North Sea. Seafloor investigations show that >7000 pockmarks are present in a ~600 km^2 area. A similar density of pockmarks is likely present over a 15,000 km^2 region outside our study area. Based on extensive monitoring, coring, geophysical and geochemical analyses, no indications of active gas seepage were found. Still, geochemical data from carbonate blocks collected from these pockmarks indicate a methanogenic origin linked to gas hydrate dissociation and past fluid venting at the seafloor. We have dated the carbonates using the U-Th method in order to constrain the pockmark formation. The carbonates gave an isochron age of 9.59 ± 1.38 ka BP, i.e. belonging to the initial Holocene. Moreover, radiocarbon dating of microfossils in the sediments inside the pockmarks is consistent with the ages derived from the carbonates. Based on pressure and temperature modelling, we show that the last deglaciation could have triggered dissociation

of gas hydrates present in the region of the northern part of the Norwegian Channel, causing degassing of 0.26 Mt_{CH4}/km^2 at the seafloor. Our results stress the importance of external climatic forcing of the dynamics of the seafloor, and the role of the rapid warming following the Younger Dryas in pacing the marine gas hydrate reservoir.

Keywords: Norwegian North Sea; Troll; pockmarks; gas hydrates dissociation; deglaciation; modelling

1. Introduction

Despite several decades of research on pockmarks, many features and mechanisms controlling their activity remain poorly understood. Key aspects such as 1) timing of formation and 2) external (climatic) versus internal (overpressure) forcing are still debated. Part of the reason for this is the limited availability of large-scale high resolution bathymetry and monitoring data from continental margins, and the lack of accurate pockmark ages.

Pockmarks often display gas flares, gas-rich sediments, gas hydrate deposits or contain carbonates originating from the seepage of thermogenic or microbial methane (e.g. Mazzini et al., 2005; Haas et al., 2010; Nickel et al., 2013). They have been found in a large variety of geological settings at continental margins (e.g. Gontharet *et al.*, 2007; Greinert *et al.*, 2010; Kocherla *et al.*, 2015). Although exceptions exist, it is commonly accepted that the driving force for pockmark formation is linked to methane migration and degassing. The methane may ultimately be sourced from deep hydrocarbon-rich reservoirs or from dissociating shallow gas hydrate deposits (e.g. Solheim and Elverhøi, 1993; Naehr *et al.*, 2000; Smith *et al.*, 2014). A common assumption is that some of the pockmarks offshore Norway were formed at some stage after the Last Glacial Maximum (e.g., about 21 ka ago), maybe even

quite recently (e.g. Jung and Vogt, 2004; Paull *et al.*, 2008; Hustoft *et al.*, 2009; Plaza-Faverola *et al.*, 2011). Cremiere *et al.* (2016) recently published a study on pockmarks in the Barents Sea, where methanogenic carbonates from pockmarks were dated. The results suggest methane seepage between 17-2 ka, linked to initial gas hydrates dissociation after the deglaciation of the southwest Barents Sea (~18–16 ka).

By investigating one of the World's largest pockmark fields offshore Norway, located above a giant gas reservoir (Fig. 1A), we aim at resolving if the degassing was driven by deep or external forcing, and if the last deglaciation was the ultimate pockmark trigger. The main difference between this study and those previously done in the same region (e.g. Vogt *et al.*, 1994; Bunz *et al.*, 2005; Mazzini *et al.*, 2006; Ivanov *et al.*, 2010; Reiche *et al.*, 2011; Chand *et al.*, 2012), is that we have access to petroleum industry data including seismic profiles and bathymetry, ROV video observations and cores and sea floor carbonate samples, providing the necessary regional coverage, and statistical analyses in addition to stratigraphic details from a selection of pockmarks.

2. Study area and Quaternary geology

The Norwegian Channel is a distinct trough separating the Norwegian mainland from the shallower parts of the North Sea Shelf to the south and west. The water depths in the central part of the trough increase gently from around 305 m in the Troll area to about 400 m at the shelf break. Fast flowing ice streams are believed to have given The Norwegian Channel its characteristic physiography (Sejrup et al., 2003; Ottesen et al., 2005). During the LGM, ice streams probably extended all the way to the shelf edge where the North Sea Trough Mouth Fan was deposited (Nygard *et al.*, 2007). The Troll area was thus situated below an ice

stream, about 200 km from its terminus during these periods. Present day Antarctic ice streams show that analogous settings have subglacial water pressures that are approximately equivalent to the glacial overburden (e.g. Alley *et al.*, 1989) and that the ice rides on a layer of deforming sediments (deformation till). The temperature and pressure regime imposed by the presence of the ice streams provides an important constraint for understanding the possible contribution of gas hydrates to the formation of pockmarks in the Norwegian Channel.

Following the break-up of the Norwegian Channel Ice Stream, the pressure history is determined by the interaction of eustatic sea level changes and isostatic rebound. Relatively rapid Late Glacial, glacial marine sedimentation has allowed the determination of a detailed seafloor temperature history for the Troll area (Sejrup *et al.*, 2003; Sejrup *et al.*, 2004).

The base of the sediments from this period is separated from the underlying gravelly and sandy sediments (Unit L3; Saalian age) by a glacial erosion surface at 74 m depth (i.e. 8903/8904 borehole in Sejrup et al., 1995; Sejrup et al., 2003). The sediments above consist of tills, probably deformation tills, deposited by the latest Norwegian Channel Ice Stream (NCIS). The top of the till at 16.9 mbsf is crenulated by iceberg plough marks and overlain by glacial marine deposits that merge into Holocene marine deposits at ~3 mbsf.

3. Methods

3.1 Marine expeditions, petrography, and geochemical and geotechnical analyses

During the period 2005-2007 large seismic and multibeam echo-sounder surveys and several sampling campaigns were conducted over the Troll gas field in the Norwegian Channel to better understand the gas transfer processes from deeper levels to the seafloor (Fig.1A). Additional high-resolution multibeam lines, video stills, and subbottom profiler (SBP) records were later acquired during several ROV dives (some examples in Fig. 1B-C). Forty-five cores and a large collection of sea floor carbonate blocks were collected from three selected pockmark complexes (Septagram, Arch, Peanut) and the surrounding areas (e.g. Fig. 1D). The data collected at these localities is used for a broader interpretation of the whole area. Carbonates were studied using optical and electron microscopy, carbon and oxygen isotope analyses and complemented with the data presented by Mazzini *et al.* (2016). The composition of the pore waters extracted from the sediment cores was also analysed. Cone penetration tests (CPT) were performed at six locations respectively outside, on the sloping edge and inside the targeted pockmarks.

3.2 Statistical analyses

A selected region of 296 km^2 from high-resolution bathymetric data was subjected to a range of data analysis methods using PAST, v. 3.04 (Hammer *et al.*, 2001) and in-house software.

Point pattern analysis can give information about the mode, timing and structural control of pockmarks (e.g. Hammer et al., 2009; Cartwright et al., 2011; Moss et al., 2012; Hillman et al., 2015). The analysis was limited to a rectangular region south of Troll A with relatively stationary point density (3189 pockmarks). Nearest-neighbour analysis (Clark and Evans, 1954) is a simple technique using the distance from each point to its nearest neighbour. The average neighbour distance is compared with the one expected for Complete Spatial

119 Randomness (CSR). Donnelly's edge correction (Donnelly, 1978) was applied. The average
120 nearest neighbour distance is 173.0 m, compared with 152.4 expected from CSR. CSR can
121 thus be rejected at $p<0.0001$ (t test). This indicates a lateral inhibition mechanism where
122 points tend to avoid each other.

123 Nearest neighbour analysis only gives information on the local scale. To investigate point
124 density at a range of scales, Ripley's *K* analysis was applied (Ripley, 1976). The number *R(d)*
125 of points within circles of radius *d* centred on one point is computed, and averaged over all
126 points. For CSR, a quadratic *R(d)* is expected, as the number of points is proportional to area.
127 A normalized function *L(d)*, square root of *R(d)*, is expected to follow *L(d)=d* for CSR. The
128 function *L(d)-d* thus represents departure from CSR at any scale *d*. An estimate of fractal
129 dimension was obtained from the asymptotic linear slope in a log-log plot of *R(d)*. The main
130 feature of the Ripley's *K* curve (Fig. 2A) is a dip at small scales (up to ca. 250 m), indicating
131 local lateral inhibition. At larger scales, the pattern drifts towards CSR. A region of elevated
132 values, corresponding to clustering, occurs at scales from 1000 to 1500 m. The estimated
133 fractal dimension value of $D=2.0$ coincides with that of CSR (Fig. 2B), and thus does not
134 give any indication of fractal geometry as might be expected from an underlying fractal
135 pattern of faults or cracks.

136 Local alignment of points along straight lines was assessed following Amorese *et al.* (1999).
137 A rectangular blade with length 1.6 km was centred on each point, and rotated through a full
138 revolution. Point counts within these blades were compared with the expected count for CSR
139 and tested using a binomial distribution with a significance level of 0.05 (not corrected for
140 multiple comparison). The alignments were filtered using the dispersion index, mean index
141 and butterfly bow criteria of Amorese *et al.* (1999). The linear alignment analysis is shown in
142 Fig. 2C. A strong preference for NNW-SSE orientation is evident in the rose plot, with an

143 average orientation of 347 degrees (geographical), random orientation rejected at $p<0.01$
144 (Rayleigh test).

145 Morphological parameters were computed as follows. For each position in the $N=7243$ data
146 set, a square with sides 150 m was extracted from the grid data, and smoothed with a
147 Gaussian filter. The local regional depth was estimated from the median depth of the corners.
148 The depth of the pockmark was estimated as the difference between the local depth and the
149 largest depth in the square. Automatic delineation of pockmarks is difficult, because the
150 depression continues gradually into the surrounding plain. For robustness, we simply defined
151 the pockmark as the area deeper than a threshold value set to 1.3 m below the local depth.
152 The diameter/depth calculations are summarized in Fig. 2D. The pockmark was edge-
153 detected using the Canny algorithm and least squares fitted to an ellipse. Diameter was
154 computed as the geometric mean between the major and minor axes. The average orientation
155 of the major axes (Fig. 2E) is 347 degrees, the same value as for the lineaments described
156 above. Random orientation can be rejected at $p<0.0001$ (Rayleigh test).

157

158 **3.3 Preparation and TIMS U-Th analysis of carbonates**

159 The carbonate blocks collected from the pockmarks contained a large fraction of detrital
160 material and were not suitable for regular U-Th dating. We performed TIMS U-Th analysis to
161 obtain isotopic ratios of $^{230}Th/^{232}Th$, $^{238}U/^{232}Th$ and $^{234}U/^{232}Th$ for isochron plotting.

162 Sample preparation and TIMS U-Th analysis (Table 1 I) was performed at the Department of
163 Earth Science, University of Bergen. Bulk carbonate samples were crushed to <5 mm and
164 washed with water to remove clay and shell fragments. Further cleaning was done by
165 repeated treatment with an EDTA and ascorbic acid solution for gentle leaching of the outer

surface of the sample fragments. For TIMS analysis sub-samples of 1-3 g were incinerated at 500 and 900°C prior to dissolution to decompose organic matter. The material was dissolved in HNO_3 and spiked with ^{233}U, ^{236}U, and ^{229}Th. Chemical separation and purification included scavenging with Fe-precipitation, two sets of ion-exchange columns (AG-1x 8 chloride forms, 200-400 mesh) and final evaporation with H_3PO_4. U and Th were loaded separately on single filaments (5x zone refined rhenium) with graphite and measured as U^+ and Th^+ on a Finnigan MAT 262 mass spectrometer, through three different experiments with SEM ion counter jumping mode acquisition. Mass calibration was done routinely when switching from lighter elements to U, as well as an initial run of the in-house standard (B-018, Eemian speleothem). All U-Th ages are reported with 2 σ uncertainties. A standard algorithm was used to calculate the ages using the program 'TIMS-Age4U2U' (Lauritzen and Lundberg, 1998). Results include activity ratios, U and Th concentrations, and U-Th ages (Fig. 3).

3.4 Radiocarbon dating of foraminifera

Radiocarbon dating was performed on foraminifera and molluscs picked from samples selected from the different cored units, both within and outside the pockmarks (Table 2, Fig. 1D). Samples were prepared by picking monospecific sub-samples of benthic foraminifera where possible from the sand fraction. Both a mollusc and foraminifera (mostly *Nonionellina labradorica*) samples were dated at BH 102 tube 6E. Samples were analysed by Beta Analytic Inc. (Florida, USA) using AMS analyses. The 2σ error in the ages of the AMS radiocarbon dates is ± 40–50 years, where σ is the standard deviation.

3.5 Gas hydrate stability modelling at Troll

189 The TEMP/W (®-TEMP/W) software was used to model the hydrate stability at the Troll
190 location in the local uppermost 450 m of the sedimentary succession. TEMP/W is a finite
191 element software that can be used to model the thermal variations in the ground related to
192 environmental changes. The formulation allows to analyse both simple and highly complex
193 geothermal problems, with or without temperatures that result in freezing or thawing of
194 sediment moisture. For this work parameters representative of gas hydrates substituted the
195 properties of ice thus allowing to determine the stability of gas hydrates for given conditions.
196 Environmental conditions, i.e. temperature and pressure, were applied to the model for a time
197 period ranging from the LGM (22 ka b2k) until 8 ka b2k (Tables 3-4). The water pressure
198 was calculated from either subglacial conditions assuming wet based ice or, following
199 deglaciation, from a combination of eustatic sea level from Deschamps *et al.* (2012) and an
200 isostatic depression of about 110 m (also used by Sejrup *et al.*, 2003 in the Troll area) that
201 decayed logarithmically until present.

202 The subglacial temperature was assumed to be 0°C. After the time of the glacial breakup,
203 from the Norwegian Channel, seafloor temperatures were based on Sejrup *et al.* (2004).
204 However, inspection of the species contributing to the earlier part of this curve may indicate
205 that the temperatures provided by these authors are too high due to the influence of reworked
206 warm water foraminifera on the transfer functions. The temperature history we used is shown
207 by the orange curve in Fig. 4A.

208 The sedimentation history was divided into 18 discrete events since the used software did not
209 allow a continuous sedimentation history. The hydrostatic pressure at the time of deposition
210 was used to define the corresponding hydrate stability vs temperature curves (Dickens and
211 Quinby-Hunt, 1994). The seafloor temperature was applied as a boundary condition to the
212 topmost layer that had been deposited at the appropriate time step. The depositional history

213 from Lehman and Keigwin (1992) was converted to calendar years using CALIB REV7.1.0
214 (Stuiver and Reimer, 1993) and the Marine 13 calibration curve (Reimer *et al.*, 2013).

215 The heat flux was kept constant but tuned to give a thermal gradient as found at present with
216 the present day stratigraphy and a temperature at the sea floor of 7°C and 13.8°C at 200 mbsf
217 (from unpublished borehole data).

218 The thermal conductivities were calculated as a function of quartz content, porosity and
219 hydrate content. The latter was limited to 10 % of the pore volume which is similar to
220 contents found by seismic refraction experiments (i.e. Bunz et al., 2005; Westbrook et al.,
221 2008 and refs therein) in hydrate bearing areas. Table 4 shows the latent heat of formation
222 and thermal conductivity of hydrate respectively.

223 The model output does not compute the migration of gas, so the hydrate content was solely
224 based on the propagation of the appropriate thermal conditions that are controlled by the heat
225 flux, thermal conductivity and the latent heat of formation of hydrate (up to a default
226 maximum of 10% of the pore volume). The model therefore indicates whether or not there is
227 a possibility for hydrate formation and also gives the time history for temperature changes to
228 propagate through the sediment.

229

230 **4. Results**

231

232 **4.1 Mapping and statistical analyses**

233 A total of 7,243 pockmarks have been mapped from the high resolution bathymetry data
234 collected in the area above the Troll field (Fig. 1A). Statistical analyses from the selected

region of bathymetric data show that the pockmarks (Fig. 1B) have an average density of 10.8 /km^2. The structures range in size from 10 to 100 meters in diameter and are typically 6 meters deep but can exceptionally be deeper than 20 meters. Three groups can be distinguished with respect to diameter/depth ratio: deep (shafts), regular (bowls) and shallow-large (saucers) (Fig. 2D). Bathymetric data also show that there is no evidence of structural control on the location of the pockmarks. This conclusion is in agreement with statistical analysis of the pockmark distribution that shows neighbour avoidance up to a scale of hundreds of meters and no indication of fractal geometry (Fig. 2C). Statistical analyses also reveal a very pronounced NNW-SSE orientation of elongated pockmarks (Fig. 2E). This orientation coincides with the main N-S currents sweeping the area. Linear alignments of pockmarks have a similar NNW-SSE trend (Fig. 2C). Industrial data (courtesy of Statoil) show that the pockmarks field extends over a broad region of 15,000 km^2 (215 km by 70 km) in the northern part of the Norwegian Channel. The pockmark density may varies from east to west, reaching a maximum of 20/km^2. By using the measured average pockmark density of 10 to 20 per square kilometre we obtain a total number of pockmarks in the range of 150,000 to 300,000 in the region, making this one of the largest pockmark fields in the World.

4.2 Sea floor observations and analytical results

In addition to the data reported by Mazzini *et al.* (2016), further observations on pockmark activity are summarized below. Sea floor images and sampling revealed the presence of broadly distributed, exhumed carbonate blocks in the pockmarks. These carbonates have bulk $\delta^{13}C$ as low as -59.7‰ V-PDB and $\delta^{18}O$ up to 4.5‰ V-PDB. These values indicate methanogenic origin, possibly linked to gas hydrate dissociation (Mazzini *et al.*, 2016) as similarly concluded from carbonate studies collected at other comparable sites (Bohrmann *et*

al., 1998; Mazzini *et al.*, 2006; Ivanov *et al.*, 2010; Cremiere *et al.*, 2016). The origin of the pockmarks can therefore be linked to methane seepage. We argue that the pockmarks in the Troll area are currently inactive based on:

a) No evidence of bubbles, fluid seepage, microbial colonies or other typical living chemosymbiotic assemblages observed during seafloor video dives or reported by the hydrocarbon industry surveys.

b) No free *in situ* gas has been found in any layer of the cores collected from the pockmarks.

c) Extended exposure of carbonates to sea floor resulting in abundant outer surface alteration, corrosion and pyrite oxidation.

d) Water analyses extracted from cores sampled inside and outside the pockmarks show no difference between pockmark and background pore water sulphate concentrations (Mazzini *et al.*, 2016).

e) No evidence of gas charged sediments or defined conduits is observable from the seismic data through the pockmarks.

f) Metagenomic studies of pockmark sediments do not show overabundance of methanotrophic organisms compared to normal sediments (Havelsrud *et al.*, 2012).

4.3 Dating the pockmark activity

In order to determine the timing and mechanisms for pockmark formation, TIMS U-Th dating was performed on ten authigenic carbonates samples from the Troll pockmark field. The TIMS results show high levels of ^{232}Th (Table 1A), and the individual U-Th analyses cannot provide reliable ages because of the detrital contamination. To resolve the contamination

281 issue we used isochron plotting to obtain the detrital-free $^{230}Th/^{234}U$ and $^{234}U/^{238}U$ ratios (Fig.
282 3, Table 1B). The best-fitted isochron plot for the Troll samples (n=5) gives a U-Th age of
283 9.59 ± 1.38 ka (Fig. 4A Table 1C). This shows that the timing of methane seepage and thus
284 carbonate formation took place shortly after the end of the Younger Dryas (YD) temperature
285 anomaly (Clark *et al.*, 2012; Deschamps *et al.*, 2012). As seep carbonates typically form by
286 rapid precipitation during methane release (e.g. Luff and Wallmann, 2003), the carbonate age
287 is virtually identical to the age of the pockmark field.

288 Further support for the new age of the pockmarks formations comes from microfossil
289 radiocarbon dating of samples from units identified with the ROV sub-bottom profiler that
290 imaged sediments down to 20-35 m (Fig. 1D, Table 2). We have identified four different
291 units adjacent to the pockmarks (Fig. 1C**)**, and these are representative for the study area
292 (Haflidason *et al.*, 1998). These are: Unit a (marine deposit 3-4 m thick, fairly transparent,
293 with a well-defined base up to 10,000 ^{14}C years BP old - 11.5 cal ka BP); Unit b (10-15 m
294 thick and well-stratified glacial marine deposit); Unit c (6-7 m thick, transparent and
295 structureless deposit, with some signal-scattering intervals > 15,000 ^{14}C years BP old – 17.8
296 cal ka BP, glacial marine, perhaps reworked by iceberg ploughing); Unit d (a probable
297 deformation till giving high-amplitude reflection which inhibits deeper imaging). Units a, b
298 and c correspond to Unit L1, whereas Unit d corresponds to Unit L2 in Sejrup *et al.*, (2003)
299 and Nygard et al. (2007) that overlies Unit L3, a sandy gravelly deposit from the penultimate
300 glaciation. The pockmarks clearly cross-cut the reflections in Unit b, including the boundary
301 between Unit a and Unit b. The radiocarbon-dated foraminifera from the bottom of the
302 Septagram pockmark gives it a maximum age of about 13 ^{14}C ka BP (~15 cal ka b2k).

303 Geotechnical cone penetration tests (CPTs) show that the sediments inside the pockmarks are
304 over-consolidated compared to those present outside where normal hemipelagic compaction

occurs. Calculations indicate that up to 7 meters of sediments have been eroded from inside the pockmarks and can account for the missing part of Unit b that were likely removed during pockmark formation (Fig. 5). Analogue and modelling studies (e.g. Pau et al., 2014 and refs therein) show that currents similar to those measured on the seafloor at Troll (i.e. up to 25 cm/s) trigger substantial turbulence inside pockmarks and are capable of preventing the sedimentation of particles up to fine sand. This process also clarifies why the pockmarks are not filled and still present on the seafloor although they are inactive. The ice-rafted clasts inside the pockmarks are interpreted to be lag deposits winnowed from Unit b (a glacial marine unit) during pockmark formation.

Besides giving an indication for the time of the pockmark formation, the calculated initial $^{234}U/^{238}U$ activity ratios (Table 1A) suggest that the carbonates precipitated from pore waters with a composition different from seawater, and that the Troll samples thus have ratios more characteristic of fresh water or evolved pore waters. Waters with fresh signatures could potentially be derived from shallow aquifers in sand-silt horizons loaded with ice-derived melt water, and/or from dissociation of gas hydrates and release of low salinity waters. The latter is more consistent with the presence of methane-derived carbonates, the broad distribution of pockmarks, and the $\delta^{18}O$ values of the carbonates.

4.4 Gas hydrate stability

The regional pressure and seafloor temperature histories since the LGM were used to model the gas hydrate stability and show that changes in seafloor temperature propagate downwards within a few hundred years affecting the hydrate stability.

327 The model shows that the gas hydrates stability zone extended down to ~300 mbsf when the
328 area was covered by an ice stream, but that the stability zone was limited to Unit L3 (~75-110
329 mbsf) following glacial breakup mainly due to the drop in pressure due to loss of subglacial
330 water pressure. This unit, consisting of coarse sand and gravels, can potentially host a
331 significant amount of hydrates and remained within the stability zone until the Holocene
332 warming of the seafloor water masses (11.5 cal ka; Sejrup *et al.*, 2004) with the possible
333 exception of a period during the Allerød-Bølling period. Fig. 4B summarizes the hydrate
334 stability in this unit. If only a few percent of CO_2 is present in the methane, the whole period
335 prior to the Holocene warming is well within the stability zone. Hughes *et al.* (2016)
336 demonstrate that the deglaciation of the most of the North Sea and the Norwegian Channel
337 occurred very quickly between 19 and 18 cal ka BP. The sudden drop in pressure (points 2 to
338 3, Fig. 4B) reflects this rapid breakup of the Norwegian Channel ice stream. Even without a
339 glacially induced elevated water pressure, Unit L3 remains within the stability zone.

340 The present gas concentrations in Unit L3 and below are relatively high whereas those in the
341 overlying units are very low (Statoil unpublished data). This piece of evidence combined with
342 modelled history of hydrate stability (Fig. 4B), supports that Unit L3 was a pre Holocene
343 reservoir for gas hydrates.

344

345 **5. Discussion**

346 **5.1 Scenario for pockmark formation**

347 The observations and the multidisciplinary data collected in the Troll region provide solid
348 data to constrain the pockmark activity and formation scenario. Rapid changes in water
349 temperature occurred during the last deglaciation with shifts in seafloor temperatures of more

than 5°C within a time period of a few decades (Lehman and Keigwin, 1992; Sejrup *et al.*, 2004; Hughes *et al.*, 2016). The numerical modelling supports the concept that abrupt climatic changes that influenced global and local ice-sheet melting histories triggered the gas hydrate dissociation and methane release to seafloor. This resulted in the rapid formation of pockmarks and extensive precipitation authigenic carbonate in the conduits close to the sea floor. This sequence of events is supported by all the available data and the formation scenario involving broad clathrate dissociation is consistent with the large number of pockmarks evenly distributed over a large flat area. This situation would unlikely result from sporadic gas seepage from deeper seated reservoirs. Further supporting evidence comes by the statistical calculations and in particular by the application of the "drainage cell" model of Moss *et al.* (2012). According to these authors, neighbour avoidance may indicate a relatively shallow source and that the pockmarks formed over a relatively short period of time. The suggested 75 m deep Unit L3 is indeed a shallow candidate that was capable of releasing significant amounts of gas from clathrates dissociation.

The fact that the gas release was synchronous throughout the area is supported by the vast regional seismic survey. The data shows no evidence of buried pockmarks other than on the horizon associated with the Younger Dryas (YD), thus ruling out the possibility of earlier stages of gas venting in the region. Instead, all the pockmarks are located at the same stratigraphic level. This timeframe not only matches the output of the applied numerical model but also the U-Th dating (9.59 ± 1.38 ka BP) of the precipitated carbonates and defines a time window for the methane seepage. Additional matching evidence is provided by the dating of the sediments around and inside the pockmarks revealing the same age of the pockmarks formation.

373 Our results show that the gas hydrate dissociation was completed after the YD, during a
374 period when rapid warming is broadly documented (e.g. Alley, 2000; Alley, 2004 and refs.
375 therein). Indeed there is no evidence of gas hydrates being currently present in the Troll area,
376 which is now outside the hydrate stability zone and showing very low methane
377 concentrations in the sediments between 0-75 m below the sea floor. No active pockmarks
378 are reported in the area although numerous surveys have been performed for the oil and gas
379 industry during the development of various hydrocarbon fields. This finding is consistent
380 with the absence of post-YD methane concentration peaks in the ice cores and with the short
381 residence time (~10 years) of methane in the atmosphere (WG1, ICCP_Report 2013). We
382 conclude that the hydrate dissociation and pockmark-derived methane release represent a
383 climate-induced pacing of the seafloor temperature. Such a scenario is relevant for
384 understanding the consequences of the current warming of the oceans.

385

386 **5.2 Gas hydrates volumes**

387 For a conservative calculation of the gas volume released from the pockmarks above the Troll
388 field, we use a 30 % porosity and a 10 % saturation of the pore volume by hydrate volume
389 present before the last deglaciation in the sand and gravel rich Unit L3 over the Troll region.
390 This is consistent with values documented by various authors (i.e. Bunz et al., 2005;
391 Westbrook et al., 2008 and refs therein). Unit L3 is on average ~7 m thick, and mapped to be
392 laterally extensive in all of the Troll region and further over a large flat area of at least 15,000
393 km^2 in the northern part of the Norwegian Channel (e.g. Rise et al., 2004). The bathymetry
394 changes by only ~100 meters from Troll to the shelf edge and pockmarks are present
395 throughout the area. Using these parameters we assess a potential volume of 3.15 km^3 of gas
396 hydrates that presumably dissociated from Unit L3 in a relatively short period of time (~150

to 300 yrs). This conservative estimate would generate ~0.26 Mt_{CH4}/km^2. The released methane was likely partly oxidized in the water column. However, if rapidly released from the pockmarks, a significant fraction would have reached the atmosphere.

6. Conclusions

Based on a multidisciplinary study from the Northern North Sea, we conclude that:

- One of the World's largest pockmark fields is located in the Norwegian Channel in the Northern North Sea. More than 7000 pockmarks have been found at the sea floor in a broad region above and around the Troll gas field. The pockmark density is ~10/km^2.
- The pockmarks do not show clustering, but rather neighbor avoidance, suggesting a regional and well distributed sub-surface source of gas.
- Carbonate geochemistry and gas hydrate stability modelling shows that gas hydrate dissociation is a likely triggering mechanism for the pockmarks. None of the investigated pockmarks showed evidence for present-day activity and gas seepage.
- U-Th dating of the carbonates shows a formation during the initial Holocene, thereby indicating that the pockmarks formed as a consequence of the rapid climatic changes following the Younger Dryas.
- We conclude that external forcing was responsible for the formation of one of the World’s largest pockmark fields.

418 **Acknowledgements**

419 We are very grateful to Statoil and the Troll license partners for giving access to data used in
420 this study. AM, HHS, and SP acknowledges support from the Research Council of Norway
421 through its Centers of Excellence funding scheme, project number 223272 (CEED). The
422 research leading to these results has received funding from by the European Research
423 Council under the European Union's Seventh Framework Programme Grant agreement n°
424 308126 (LUSI LAB project, PI A. Mazzini).

425

426

427 **Figure captions**

428

429 **Fig. 1 (A)** Fragment of Troll field multibeam coverage where more than 7,000 pockmarks
430 (2.5 m gridding resolution) have been mapped. Indicated are the Troll A platform and the
431 pockmark areas more intensively studied. Inset map offshore Norway. UTM Zone 31,WGS84
432 datum. **(B)** Example of high-resolution bathymetry (0.2 m resolution) of the Septagram
433 pockmarks showing a 15 m deep circular depression with a flat interior For location refer to
434 Fig. 1A. **(C)** Example of ROV sub-bottom profile through the Septagram pockmark.
435 Indicated are the four imaged units (a-d). Fir size refer to Fig. 1B. The pockmarks typically
436 cross-cut the reflections of Unit b. See text for geochronology of these units. (**D**) Multibeam
437 line across the Septagram region and locations of the cores available that were collected in
438 the area for radiocarbon dating and CPT (pink triangles). The scale for the maps in the
439 manuscript are in meters or kilometers, UTM Zone 31, WGS84 datum.

Fig.2 (A) Ripley's *K* analysis. **(B)** Log-log plot of Ripley's *R*(*d*). The asymptotic linear slope gives a fractal dimension close to *D*=2.0. **(C)** Lineaments found with the blade method and rose plot of the orientations over the survey area (scale in kilometers). **(D)** Diameter and depth of the analysed pockmarks highlights three distinct groups of pockmarks: deep (shafts), regular (bowls) and shallow-large (saucers). **(E)** A pockmark with its fitted ellipse. Grid cells are 2.5 m square. Rose plot of major axis orientations (N=6834). The mean pockmark orientation coincides with the main N-S currents swiping the area.

Fig. 3 U-T raw data isochron plots for the Troll samples. The slopes of the regression lines provide the detrital Th-free ratios of $^{230}Th/^{234}U$ and $^{234}U/^{238}U$. The intercept with the y-axis in the left diagram gives the un-contaminated $^{230}Th/^{232}Th$ activity ratio.

Fig. 4 (A) Single age data and isochron data from all the samples compared to 1) the Greenland temperature data (GISP2 core, Alley, 2000; Alley, 2004); 2) the (GISP2 core, Alley, 2000); 2) temperature history for the hydrate stability modelling (orange curve) with some adjustments in the older parts where the transfer functions may be influenced by reworked warm species.). The orange curve is derived from 3) the seafloor temperature history from Sejrup *et al.* (2004) (black curve). The Troll carbonate ages follow the Younger Dryas rapid warming event. Carbonate formation (and hence pockmark formation) could be related to the deglaciation and the resulting changes in sea floor pressures and temperatures that followed. (B) The pressure-temperature development from Table 3 (point numbers in blue) plotted in a diagram showing the stability zone of methane hydrate (light blue area to

463 the upper left). The point numbers in Table 3 are shown in blue. The dashed red line indicates
464 the hydrate stability curve for methane with 10 % CO2.

465

466 **Fig. 5** Results of CPT tests performed in the study area. The results are adjusted to same
467 depth below sea level (i.e. elevation). The shaded area shows the range of CPT measurements
468 previously performed in the Troll area. Fig. 1D shows location of CPT stations.

469

470 **References**

471

472 ®-TEMP/W, https://www.geo-slope.com/products/temp-w.
473 Alley, R. B., 2000, The Younger Dryas cold interval as viewed from central Greenland: Quaternary
474 Science Reviews, v. 19, p. 213-226.
475 Alley, R. B., 2004, GISP2 Ice Core Temperature and Accumulation Data: IGBP PAGES/World Data
476 Center for Paleoclimatology Data Contribution Series #2004-013. NOAA/NGDC
477 Paleoclimatology Program, Boulder CO, USA.
478 Alley, R. B., Blankenship, D. D., Rooney, S. T., and Bentley, C. R., 1989, Water-pressure coupling of
479 the sliding and bed deformation: III. Application to Ice Stream B, Antarctica: Journal of
480 Glaciology, v. 35, p. 130-139.
481 Amorese, D., Lagarde, J.-L., and Laville, E., 1999, A point pattern analysis of the distribution of
482 earthquakes in Normandy (France): Bulletin of the Seismological Society of America v. 89, p.
483 742-749.
484 Bohrmann, G., Greinert, J., Suess, E., and Torres, M., 1998, Authigenic carbonates from the Cascadia
485 subduction zone and their relation to gas hydrate stability: Geology, v. 7, p. 647-650.
486 Bunz, S., Mienert, J., Vanneste, M., and Andreassen, K., 2005, Gas hydrates at the Storegga Slide:
487 Constraints from an analysis of multicomponent, wide-angle seismic data: Geophysics, v. 70,
488 p. B19-B34.
489 Cartwright, A., Moss, J., and Cartwright, J., 2011, New statistical methods for investigating submarine
490 pockmarks: Computers & Geosciences, v. 37, p. 1595-1601.
491 Chand, S., Thorsnes, T., Rise, L., Brunstad, H., Stoddart, D., Bøe, R., Lågstad, P., and Svolsbru, T.,
492 2012, Multiple episodes of fluid flow in the SW Barents Sea (Loppa High) evidenced by gas
493 flares, pockmarks and gas hydrate accumulation: Earth and Planetary Science Letters, v.
494 331–332, p. 305-314.
495 Clark, P. J., and Evans, F. C., 1954, Distance to nearest neighbour as a measure of spatial patterns in
496 biological populations.: Ecology v. 35, p. 445-453.
497 Clark, P. U., et al., 2012, Global climate evolution during the last deglaciation: Proceedings of the
498 National Academy of Sciences, v. 109, p. E1134-E1142.

499 Cremiere, A., et al., 2016, Timescales of methane seepage on the Norwegian margin following
500 collapse of the Scandinavian Ice Sheet: Nat Commun, v. 7.
501 Deschamps, P., Durand, N., Bard, E., Hamelin, B., Camoin, G., Thomas, A. L., Henderson, G. M.,
502 Okuno, J., and Yokoyama, Y., 2012, Ice-sheet collapse and sea-level rise at the Bolling
503 warming 14,600 years ago: Nature, v. 483, p. 559-564.
504 Dickens, G. R., and Quinby-Hunt, M. S., 1994, Methane hydrate stability in seawater: Geophysical
505 Research Letters, v. 21, p. 2115-2118.
506 Donnelly, K., 1978, Simulations to determine the variance and edge-effect of total nearest neighbour
507 distance., *in* Hodder, I., ed., Simulation Methods in Archaeology, Cambridge University Press,
508 London.
509 Gontharet, S., Pierre, C., Blanc-Valleron, M. M., Rouchy, J. M., Fouquet, Y., Bayon, G., Foucher, J. P.,
510 Woodside, J., and Mascle, J., 2007, Nature and origin of diagenetic carbonate crusts and
511 concretions from mud volcanoes and pockmarks of the Nile deep-sea fan (eastern
512 Mediterranean Sea): Deep Sea Research Part II: Topical Studies in Oceanography, v. 54, p.
513 1292-1311.
514 Greinert, J., Bialas, J., Lewis, K., and Suess, E., 2010, Methane seeps at the Hikurangi Margin, New
515 Zealand: Marine Geology, v. 272, p. 1-3.
516 Haas, A., Peckmann, J., Elvert, M., Sahling, H., and Bohrmann, G., 2010, Patterns of carbonate
517 authigenesis at the Kouilou pockmarks on the Congo deep-sea fan: Marine Geology, v. 268,
518 p. 129-136.
519 Haflidason, H., King, E. L., and Sejrup, H. P., 1998, Late Weichselian and Holocene sediment fluxes of
520 the northern North Sea Margin: Marine Geology, v. 152, p. 189-215.
521 Hammer, Ø., Harper, D. A. T., and Ryan, P. D., 2001, PAST: Palaeontological Statistics software
522 package for education and data analysis: Palaeontologia Electronica v. 4, p. 9.
523 Hammer, Ø., Webb, K., and Depreiter, D., 2009, Numerical simulation of upwelling currents in
524 pockmarks, and data from the Inner Oslofjord, Norway: Geo-Marine Letters, v. 29, p. 269-
525 275.
526 Havelsrud, O. E., Haverkamp, T. H. A., Kristensen, T., Jakobsen, K. S., and Rike, A. G., 2012,
527 Metagenomic and geochemical characterization of pockmarked sediments overlaying the
528 Troll petroleum reservoir in the North Sea: Bmc Microbiology, v. 12.
529 Hillman, J. I. T., Gorman, A. R., and Pecher, I. A., 2015, Geostatistical analysis of seafloor depressions
530 on the southeast margin of New Zealand's South Island - Investigating the impact of dynamic
531 near seafloor processes on geomorphology: Marine Geology v. 360, p. 70-83.
532 Hughes, A. L. C., Gyllencreutz, R., Lohne, Ø. S., Mangerud, J., and Svendsen, J. I., 2016, The last
533 Eurasian ice sheets – a chronological database and time-slice reconstruction, DATED-1:
534 Boreas, v. 45, p. 1-45.
535 Hustoft, S., Dugan, B., and Mienert, J., 2009, Effects of rapid sedimentation on developing the
536 Nyegga pockmark field: Constraints from hydrological modeling and 3-D seismic data,
537 offshore mid-Norway: Geochemistry, Geophysics, Geosystems, v. 10, p. Q06012.
538 Ivanov, M., Mazzini, A., Blinova, V., Kozlova, E., Laberg, J.-S., Matveeva, T., Taviani, M., and Kaskov,
539 N., 2010, Seep mounds on the Southern Vøring Plateau (offshore Norway): Marine and
540 Petroleum Geology, v. 27, p. 1235-1261.
541 Jung, W.-Y., and Vogt, P. R., 2004, Effects of bottom water warming and sea level rise on Holocene
542 hydrate dissociation and mass wasting along the Norwegian-Barents Continental Margin: J.
543 Geophys. Res. Solid Earth, v. 109, B06104.
544 Kocherla, M., Teichert, B. M. A., Pillai, S., Satyanarayanan, M., Ramamurty, P. B., Patil, D. J., and Rao,
545 A., 2015, Formation of methane-related authigenic carbonates in a highly dynamic
546 biogeochemical system in the Krishna–Godavari Basin, Bay of Bengal: Marine and Petroleum
547 Geology, v. 64, p. 324-333.

548 Lauritzen, S.-E., and Lundberg, J., 1998, TIMS-Age4U2U. Program for data reduction of TIMS U-series
549 Dating. Code and algorithms, Version 2.3: Department of Geology, University of Bergen,
550 Norway.
551 Lehman, S. J., and Keigwin, L. D., 1992, Sudden Changes in North-Atlantic Circulation during the Last
552 Deglaciation: Nature, v. 356, p. 757-762.
553 Luff, R., and Wallmann, K., 2003, Fluid flow, methane fluxes, carbonate precipitation and
554 biogeochemical turnover in gas hydrate-bearing sediments at Hydrate Ridge, Cascadia
555 Margin: numerical modeling and mass balances: Geochimica et Cosmochimica Acta, v. 67, p.
556 3403-3421.
557 Mazzini, A., Aloisi, G., Akhmanov, G. G., Parnell, J., Cronin, B., and Murphy, P., 2005, Integrated
558 petrographic and geochemical record of hydrocarbon seepage on the Vøring Plateau:
559 Geological Society, v. 162, p. 815-827.
560 Mazzini, A., Svensen, H., Hovland, M., and Planke, S., 2006, Comparison and implications from
561 strikingly different authigenic carbonates in a Nyegga complex pockmark, G11, Norwegian
562 Sea: Marine Geology, v. 231, p. 89-102.
563 Mazzini, A., Svensen, H. H., Planke, S., Forsberg, C. F., and Tjelta, T. I., 2016, Pockmarks and
564 methanogenic carbonates above the giant Troll gas field in the Norwegian North Sea: Marine
565 Geology, v. 373, p. 26-38.
566 Moss, J. L., Cartwright, J., Cartwright, A., and Moore, R., 2012, The spatial pattern and drainage cell
567 characteristics of a pockmark field, Nile Deep Sea Fan: Marine and Petroleum Geology v. 35,
568 p. 321-336.
569 Naehr, T. H., Rodriguez, N. M., Bohrmann, G., Paull, C. K., and Botz, R., 2000, Methane-derived
570 authigenic carbonates associated with gas hydrate decomposition and fluid venting above
571 the Blake Ridge Diapir, *in* Paull, C. K., Matsumoto, R., Wallace, P. J., and Dillon, W. P., eds.,
572 Proc. ODP Scientific Results, Volume 164, College Station, TX (Ocean Drilling Program), p.
573 286-300.
574 Nickel, J. C., di Primio, R., Kallmeyer, J., Hammer, Ø., Horsfield, B., Stoddart, D., Brunstad, H., and
575 Mangelsdorf, K., 2013, Tracing the origin of thermogenic hydrocarbon signals in pockmarks
576 from the southwestern Barents Sea: Organic Geochemistry, v. 63, p. 73-84.
577 Nygard, A., Sejrup, H. P., Haflidason, H., Lekens, W. A. H., Clark, C. D., and Bigg, G. R., 2007, Extreme
578 sediment and ice discharge from marine-based ice streams: New evidence from the North
579 Sea: Geology, v. 35, p. 395-398.
580 Ottesen, D., Rise, L., Knies, J., Olsen, L., and Henriksen, S., 2005, The Vestfjorden-Trænadjupet
581 palaeo-ice stream drainage system, mid-Norwegian continental shelf: Marine Geology, v.
582 218, p. 175-189.
583 Pau, M., Gisler, G., and Hammer, Ø., 2014, Experimental investigation of the hydrodynamics in
584 pockmarks using particle tracking velocimetry: Geo-Marine Letters, v. 34, p. 11-19.
585 Paull, C., et al., 2008, Origin of pockmarks and chimney structures on the flanks of the Storegga Slide,
586 offshore Norway: Geo-Marine Letters, v. 28, p. 43-51.
587 Plaza-Faverola, A., Bünz, S., and Mienert, J., 2011, Repeated fluid expulsion through sub-seabed
588 chimneys offshore Norway in response to glacial cycles: Earth and Planetary Science Letters,
589 v. 305, p. 297-308.
590 Reiche, S., Hjelstuen, B. O., and Haflidason, H., 2011, High-resolution seismic stratigraphy,
591 sedimentary processes and the origin of seabed cracks and pockmarks at Nyegga, mid-
592 Norwegian margin: Marine Geology, v. 284, p. 28-39.
593 Reimer, P. J., et al., 2013, Intcal13 and Marine13 Radiocarbon Age Calibration Curves 0-50,000 Years
594 Cal Bp: Radiocarbon, v. 55, p. 1869-1887.
595 Ripley, B. D., 1976, The second-order analysis of stationary point processes: Journal of Applied
596 Probability v. 13, p. 255-266.

Rise, L., Olesen, O., Rokoengen, K., Ottesen, D., and Riis, F., 2004, Mid-Pleistocene ice drainage pattern in the Norwegian Channel imaged by 3D seismic: Quaternary Science Reviews, v. 23, p. 2323-2335.

Sejrup, H. P., Aarseth, I., Hafiidason, H., Løvlie, R., Bratten, Å., Tjøstheim, G., Forsberg, C. F., and Ellingsen, K. L., 1995, Quatemary of the Norwegian Channel: glaciation history and palaeoceanography: Norsk Geologisk Tidsskrift, v. 75, p. 65-87.

Sejrup, H. P., Birks, H. J. B., Kristensen, D. K., and Madsen, H., 2004, Benthonic foraminiferal distributions and quantitative transfer functions for the northwest European continental margin: Marine Micropaleontology, v. 53, p. 197-226.

Sejrup, H. P., et al., 2003, Configuration, history and impact of the Norwegian Channel Ice Stream: Boreas, v. 32, p. 18-36.

Smith, A. J., Mienert, J., Bunz, S., and Greinert, J., 2014, Thermogenic methane injection via bubble transport into the upper Arctic Ocean from the hydrate-charged Vestnesa Ridge, Svalbard: Geochemistry Geophysics Geosystems, v. 15, p. 1945-1959.

Solheim, A., and Elverhøi, A., 1993, Gas-related sea floor craters in the Barents Sea: Geo Marine Letters, v. 13, p. 235-243.

Stuiver, M., and Reimer, P. J., 1993, Extended 14C database and revised CALIB radiocarbon calibration program: Radiocarbon v. 35, p. 215-230.

Vogt, P. R., Crane, K., Sundvor, E., Max, M. D., and Pfirman, S. L., 1994, Methane-Generated (Questionable) Pockmarks on Young, Thickly Sedimented Oceanic-Crust in the Arctic - Vestnesa-Ridge, Fram Strait: Geology, v. 22, p. 255-258.

Westbrook, G. K., et al., 2008, Estimation of gas hydrate concentration from multi-component seismic data at sites on the continental margins of NW Svalbard and the Storegga region of Norway: Marine and Petroleum Geology, v. 25, p. 744-758.

WG1, ICCP_Report 2013, Climate change 2013, The Physical Science Basis: ICCP_Report, v. Fifth Assesment Report.

Figure1

Click here to download Figure: Fig_1_troll2_modif.pdf

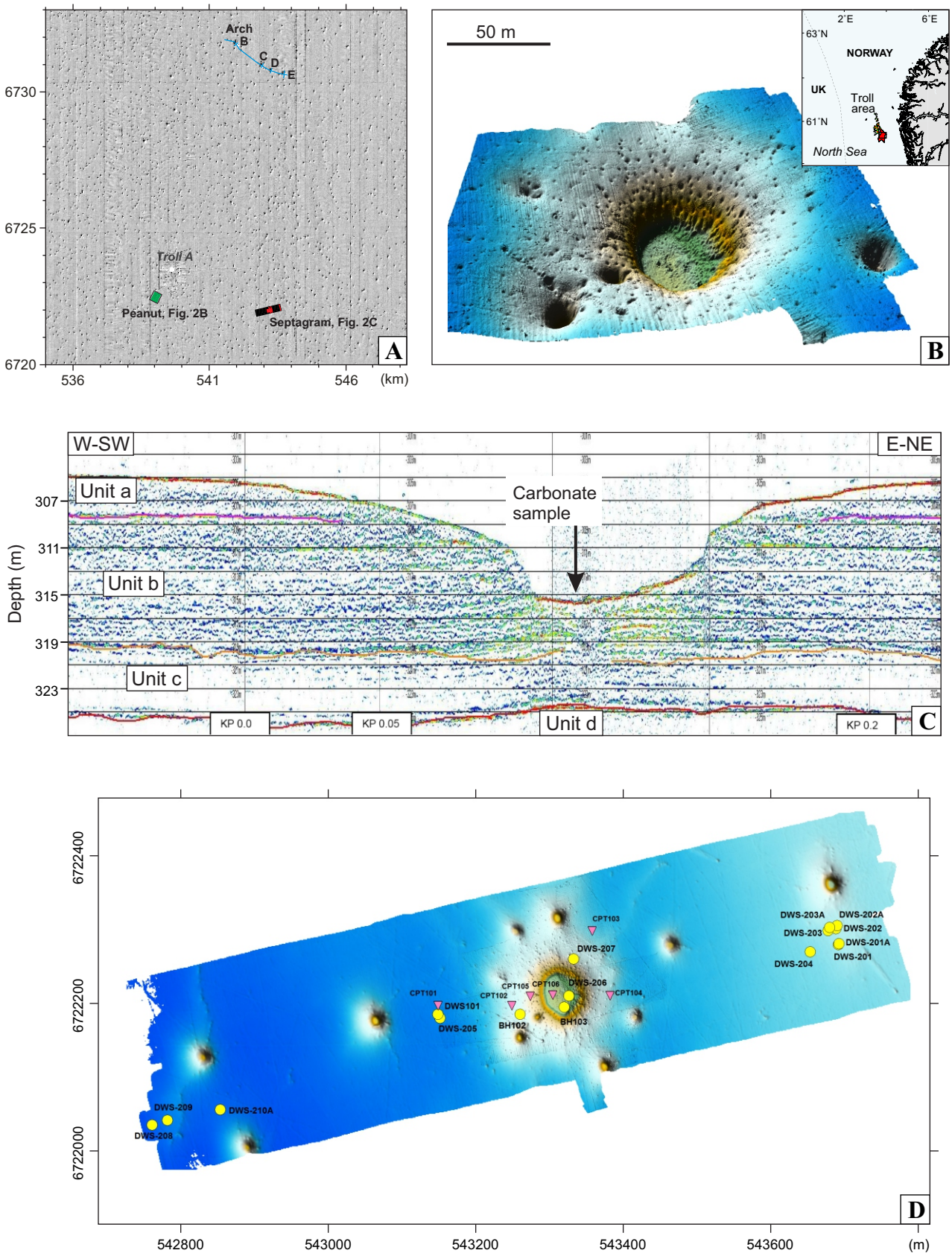

Figure2

Click here to download Figure: Fig_2_troll2.pdf

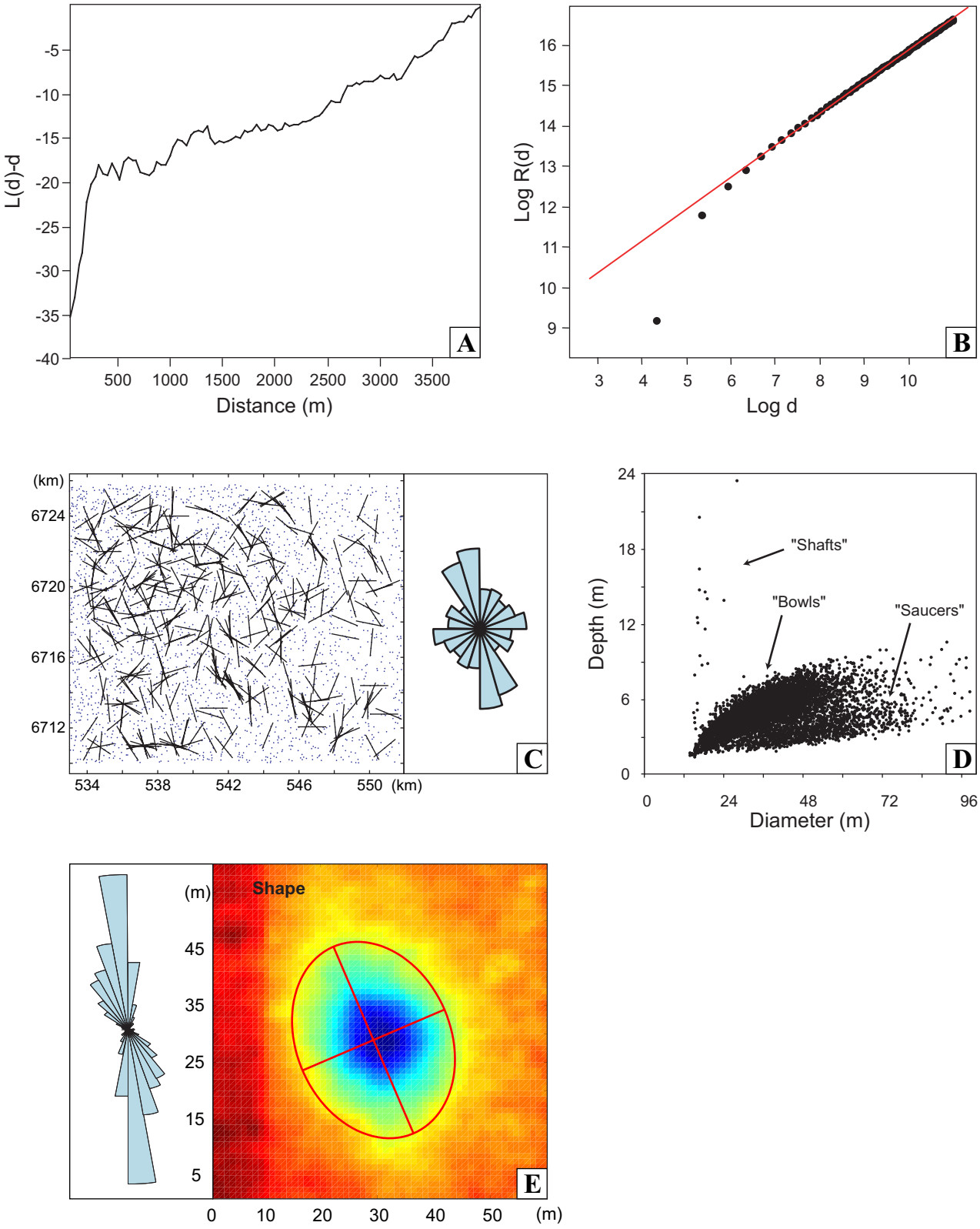

Figure3

Click here to download Figure: Fig_3_troll2.pdf

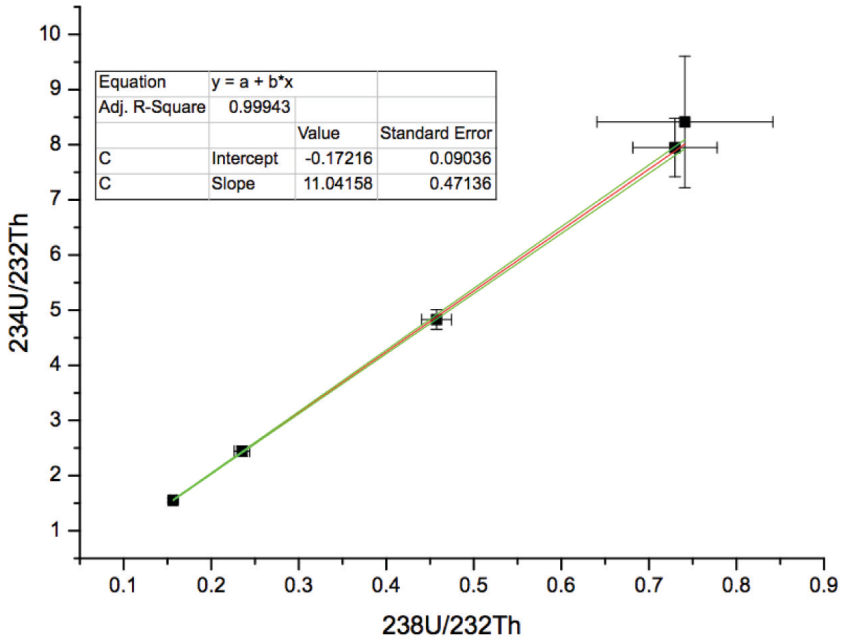

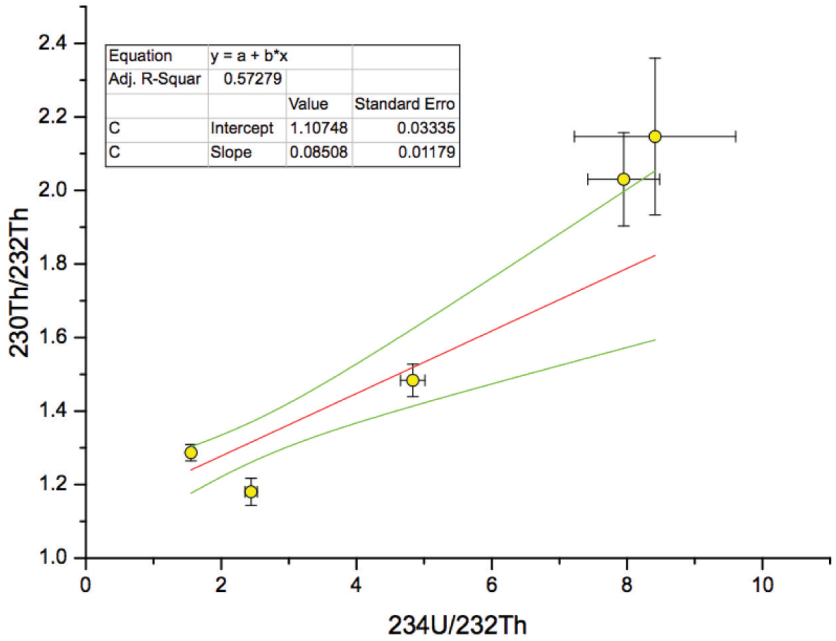

Figure4

Click here to download Figure: Fig_4_troll2.pdf

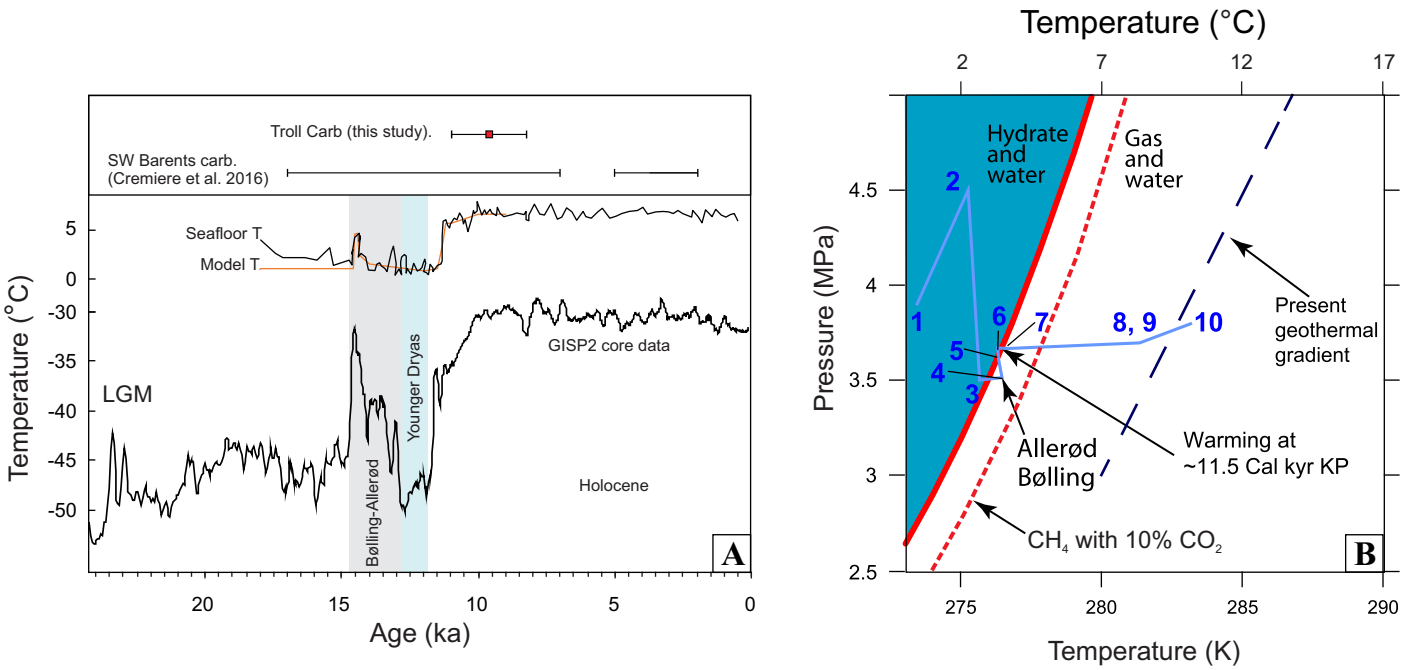

Figure5

Click here to download Figure: Fig_5_troll2.pdf

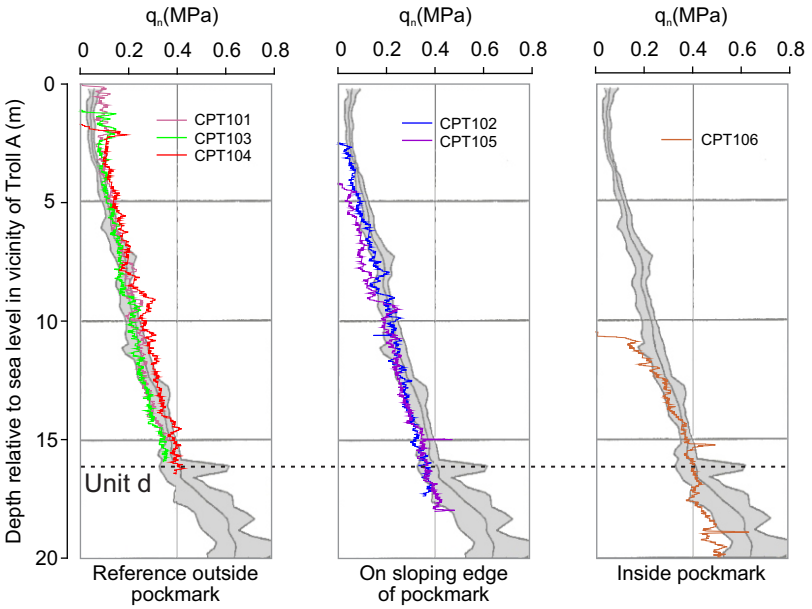

Table1

Click here to download Table: Table1_HL_070316.pdf

Table 1.

I - Summarised output of TIMS U-Th analysis of pockmark carbonates from Septagram, Troll. All errors are 2σ.

Lab.No.	Sample ID	ppm ^{238}U	ppm ^{232}Th	$^{234}U/^{238}U$ (act)	$^{230}Th/^{234}U$ (act)	$^{230}Th/^{232}Th$ (act)	$^{234}U/^{238}U$ (init act)	Age ± 2σ (ka)	Corrected age (ka)*
716	B53-2 mørk	4.128 ± 0.019	154	1.126 ± 0.018	0.255 ± 0.006	2.030 ± 0.127	1.14 ± 0.02	31.89 ± 0.89	9.31 ± 1.92
717	B53-2 lys	3.986 ± 0.078	147	1.173 ± 0.081	0.255 ± 0.026	2.147 ± 0.213	1.19 ± 0.08	31.80 ± 3.90	10.65 ± 3.79
732	B67-4	1.024 ± 0.003	182	1.026 ± 0.010	0.828 ± 0.012	1.289 ± 0.022	1.04 ± 0.01	188.3 ± 8.8	Negative§
733	B67-6	1.527 ± 0.005	178	1.073 ± 0.011	0.483 ± 0.010	1.180 ± 0.037	1.09 ± 0.01	71.18 ± 2.18	Negative§
734	B610-8	2.438 ± 0.008	145	1.091 ± 0.009	0.307 ± 0.007	1.484 ± 0.044	1.10 ± 0.01	39.67 ± 1.08	Negative§

* Correction factor used by TIMS Age4U2U (Lauritzen and Lundberg, 1998) is 1.5. § Negative because correction factor is larger than present-day measured value

II – Ratios for isochron plotting calculated from TIMS U-Th analysis. All errors are 2σ.

Lab.No.	$^{230}Th/^{232}Th$	$^{238}U/^{232}Th$	$^{234}U/^{232}Th$
716	2.0303 ± 0.1268	0.7298 ± 0.0482	7.9493 ± 0.5300
717	2.1468 ± 0.2132	0.7410 ± 0.1005	8.4132 ± 1.1927
732	1.2868 ± 0.0223	0.1565 ± 0.0034	1.5546 ± 0.0355
733	1.1803 ± 0.0369	0.2352 ± 0.0088	2.4414 ± 0.0916
734	1.4835 ± 0.0441	0.4575 ± 0.0171	4.8314 ± 0.1790

III – Activity ratios for calculating ^{230}Th ages and resulting ages (± 1σ).

Group	$^{234}U/^{238}U$	$^{230}Th/^{234}U$	Age ± 1σ (ka)
Troll – Septagram	11.042 ± 0.471	0.08508 ± 0.01179	9.587 + 1.378 – 1.366

Table2

Click here to download Table: Table 2 14C_age_table_26.02.2016_v3-1.pdf

Table 2: Results of radiocarbon analyses and core coordinates.

Name	Sample	Northings	Eastings	Depth (m)	Dated material	^{14}C Age (yrs)	St.dv. (1 s)	d^{13}C ‰ (V-PDB)	Cal age b2k	Cal age (1 s)
BH102	BH 102 tube 6E	6722185	543260	5.80	*Molluscs*	12 430	40	-0.8	13 960	70
BH102	BH 102 tube 6E	6722185	543260	5.80	*N. labradorica*	12 960	50	-4.8	14 955	150
BH103	BH 103 tube 7	6722195	543320	6.40	*N. labradorica*	14 290	50	-2.4	16 890	130
DWS101	DWS 101 tube 7	6722185	543149	10.00	*N. labradorica*	13 180	40	-10.4	15 270	70
DWS-201A	DWS 201A-2-D	6722280.8	543691.8	0.64	*U. mediterranea*	6 020	40	-0.3	6 490	55
DWS-201A	DWS 201A-5-B/C	6722280.8	543691.8	3.39	*U. mediterranea*	9 950	40	-1.8	10 980	95
DWS-201A	DWS 201-A-Shoe B	6722280.8	543691.8	5.43	*N. labradorica*	11 160	40	-2.4	12 710	45
DWS-204	DWS 204-4-F	6722269.7	543653.1	2.90	*N. labradorica*	11 140	40	-3.4	12 700	45
DWS-204	DWS 204-6-B	6722269.7	543653.1	4.47	Sp. Undetermined	11 790	40	-0.8	13 320	55
DWS-206	DWS 206-2-D	6722210.2	543326.4	0.45	*N. labradorica*	12 980	40	-3.2	14 995	130
DWS-209	DWS 209-3-F	6722041.7	542782.8	1.25	*U. mediterranea*	7 300	40	-0.2	7 810	55
DWS-209	DWS 209-6-B	6722041.7	542782.8	3.75	*N. labradorica*	10 940	40	-4	12 570	60
DWS-209	DWS 209-6H	6722041.7	542782.8	4.55	*N. labradorica*	12 130	40	-3.2	14 205	75
DWS-209	DWS 209-6H	6722041.7	542782.8	4.55	*N. labradorica*	12 090	40	-1.4	13 575	70

Table3
Click here to download Table: Table3.pdf

Table 3: Pressure and temperature development for moraine layer (Unit L3) at 90 mbsf. The temperatures have been extracted from model. The pressure was calculated from a combination of water depth (Fleming et al, 1998) and estimated isostatic depression for points 3 to 7. For points 1 and 2 a subglacial water pressure corresponding to a head of water of 200 m water above sea level was used. All hydrate had melted for points 8, 9 and 10. Point no. refers to blue number in Fig. 4B.

Point No.	**Temp.** (°K)	**Pressure** (MPa)	**Cal Age** (ka BP)	**Rel. Sea level** (m)	**Isostasy** (m)	**'Seafloor" temp** (°K)	**Burial depth** (m)	**Comment**
1	273.5	3.9	22	-110	100	273	6	Ice Stream: 200 m head of water
2	275.4	4.5	18.5	-93	100	273	62	Burial by till: 200 m head of water
3	275.7	3.5	16.5	-93	63	274	62	Cold seafloor water at site. Ice breaks up – no sub glacial pressure.
4	276.6	3.55	14.3	-73	48	274	64	Allerød warming
5	276.35	3.62	13.5	-63	45	274	72	Burial, rising sea level
6	276.35	3.67	11.5	-45	32	274	76.5	End of ice age
7	276.64	3.67	11.3	-45	32	277	76.5	Influx of warm water
8	281.35	3.9	8.5	-13	23	277	77.8	Rising sea level
9	281.35	3.9	8.5	-13	23	280	77.8	Warmer water
10	283.14	3.8	0	0	0	280	80	Present

Table 4. Properties of water and hydrate used to calculate the thermal properties of the sediments.

Parameter	**Value**	**Unit**
Seawater density	1027	$kg \cdot m^{-3}$
Hydrate density	915	$kg \cdot m^{-3}$
Grain matrix density	2793.44	$kg \cdot m^{-3}$
Thermal conductivity of seawater	49.68	$kJ \cdot days^{-1} \cdot m^{-1} \cdot K^{-1}$
Thermal conductivity of hydrate	42.34	$kJ \cdot days^{-1} \cdot m^{-1} \cdot K^{-1}$
Thermal conductivity of quartz	664.42	$kJ \cdot days^{-1} \cdot m^{-1} \cdot K^{-1}$
Thermal conductivity of non-quartz minerals	216	$kJ \cdot days^{-1} \cdot m^{-1} \cdot K^{-1}$
Quartz fraction of grains	0.2	-
Specific heat capacity of seawater	3.87	$kJ \cdot kg^{-1} \cdot K^{-1}$
Specific heat capacity of hydrate	2.08	$kJ \cdot kg^{-1} \cdot K^{-1}$
Specific heat capacity of grains	0.71	$kJ \cdot kg^{-1} \cdot K^{-1}$
Volumetric heat capacity of seawater	3974.49	$kJ \cdot m^{-3} \cdot K^{-1}$
Volumetric heat capacity of hydrate	1903.2	$kJ \cdot m^{-3} \cdot K^{-1}$
Volumetric heat capacity of grains	1983.34	$kJ \cdot m^{-3} \cdot K^{-1}$
Latent heat of hydrate	430	$kJ \cdot kg^{-1}$
Volumetric latent heat of hydrate	393450	$kJ \cdot m^{-3}$